Proceedings of ASME Turbo Expo 2011
GT2011
June 6-10, 2011, Vancouver, British Columbia, Canada

GT2011-46555

OPTIMIZATION OF A U-BEND FOR MINIMAL PRESSURE LOSS IN INTERNAL COOLING CHANNELS – PART II: EXPERIMENTAL VALIDATION

Filippo Coletti, Tom Verstraete, Timothée Vanderwielen, Jérémy Bulle, Tony Arts

von Karman Institute for Fluid Dynamics
Turbomachinery and Propulsion Department
Chaussée de Waterloo 72
1640 Rhode-Saint-Genèse, Belgium
Email: coletti@vki.ac.be
tom.verstraete@vki.ac.be

ABSTRACT

This two-part paper addresses the design of a U-bend for serpentine internal cooling channels optimized for minimal pressure loss. The total pressure loss for the flow in a U-bend is a critical design parameter as it augments the pressure required at the inlet of the cooling system, resulting in a lower global efficiency. In the first part of the paper the design methodology of the cooling channel was presented. In this second part the optimized design is validated.

The results obtained with the numerical methodology described in Part I are checked against pressure measurements and Particle Image Velocimetry (PIV) measurements. The experimental campaign is carried out on a magnified model of a two-legged cooling channel that reproduces the geometrical and aerodynamical features of its numerical counterpart. Both the original profile and the optimized profile are tested. The latter proves to outperform the original geometry by about 36%, in good agreement with the numerical predictions. Two-dimensional PIV measurements performed in planes parallel to the plane of the bend highlight merits and limits of the computational model. Despite the well-known limits of the employed eddy viscosity model, the overall trends are captured.

The study demonstrates that the proposed optimization method based on an evolutionary algorithm, a Navier-Stokes solver and a meta-model of it is a valid design tool to minimize the pressure loss across a U-bend in internal cooling channels.

INTRODUCTION

State-of-the-art gas turbines are designed to operate at turbine inlet temperatures that approach 2000 K. Since the materials commonly employed for the turbine components cannot withstand temperatures above 1350 K, effective cooling must be applied along the hot-gas-path in order to guarantee safe functioning. Typically the coolant is air bled from the high pressure compressor, which bypasses the combustor and enters the blade through its root, circulating through serpentine internal passages. More than 20% of the discharge air from the compressor is used to cool the high pressure turbine, leading to a severe penalty on the thermodynamic efficiency. An effective design must maintain the metal temperature below acceptable limits with minimal coolant mass flow rates and pressure drop penalties. Reviews of turbine blade cooling techniques were presented by Han et al. [1] and Weigand et al. [2].

Among the salient features of the cooling passages, the U-bends that connect consecutive channels play a key role, as they represent regions of strong pressure loss. Numerous experiments investigating the turbulent flow in 180° bends have been conducted. The contributions of Humphrey et al. [3], Chang et al. [4], Monson and Seegmiller [5] and Cheah et al. [6] using laser Doppler velocimetry (LDV) concern circular U-bends. The velocity field in sharp corner bends was investigated by Liou and Chen [7] by LDV, Son et al. [8] by two-dimensional particle image velocimetry (PIV) and Schabacker et al. [9] by stereoscopic PIV. All studies highlighted the presence of secondary flows driven by the imbalance between the centrifugal forces and the radial pressure gradient.

U-bend geometries make an excellent test case for turbulence models, as the effects of the streamline curvature and the associated secondary flows are typically challenging to reproduce in numerical simulations. The broad trends can be captured by two-equation eddy-viscosity models, provided that the boundary layer is resolved without recurring to wall functions, as discussed by Iacovides and Launder [10].

However two-equation models cannot predict the effect of streamline curvature on the turbulence structure due to their inability to account for turbulence anisotropy. Nevertheless, due to their reduced computational cost, two-equation models are still the standard tool in industrial applications.

The high pressure penalty imposed by the U-bend has fostered the interest towards strategies to improve their aerodynamic performance, especially in sharp turn configurations. Metzger et al. [11] varied the width of the passages, the corner radius and the clearance height. The influence of the dividing wall thickness was explored by Liou and Chen [12]. Bonhof et al. [13] showed that inserting turning vanes alleviates the pressure loss.

All the above-mentioned studies concerned with the minimization of the U-bend pressure drop follow a classic trial-and-error approach: several configurations are generated varying a number of geometrical parameters, performances are compared and global trends are evaluated. However, given the large number of parameters, this type of design process remains extremely time-consuming. Moreover, as many of the parameters are strongly coupled, the relations between them and their effects are difficult to asses. In order to ease and speed up the process, the so called optimization methods can be applied. Most of these techniques exploit natural principles to obtain effective solutions, while minimizing the intervention of the human designer. A recent example is the study of Zehner et al. [14], who optimized the dividing wall of a sharp U-bend. They used the ice-formation technique to generate a starting profile of minimum energy dissipation, and further improved the performance applying an evolutionary algorithm. Namgoong et al. [15] used Design of Experiment and surrogate design space model for similar purposes.

The present two-part paper addresses the design of a smooth U-bend of radius ratio 0.76, optimized for minimal pressure loss. The considered duct has a square cross section and the two legs are connected by a simple 180° semi-circular curve. In the first part of the paper [16] the design methodology, based on an evolutionary algorithm, a Navier-Stokes solver and a meta-model of it, has been presented. In this second part, the results obtained with such a methodology are compared with pressure measurements and Particle Image Velocimetry (PIV) measurements performed on real models that replicate the original circular U-bend and the optimized bend. The results in terms of pressure drop are interpreted in light of the velocity fields, allowing to assess the reliability of the proposed design tool.

EXPERIMENTAL APPARATUS AND PROCEDURES

Set up and operating conditions

The measurement campaign is conducted on large scale models that replicate the geometrical features and the aerodynamic conditions of the numerical models presented in Part I. The experimental set-up is sketched in Fig. 1. The air flow is regulated by a 2.2 kW centrifugal blower discharging into a settling chamber. The latter is equipped with a honeycomb which minimizes the swirl of the flow generated by the blower. The air in the settling chamber is seeded with tracer particles (1 to 6 microns in diameter) obtained vaporizing oil in a smoke generator. The air streams then through the test section, which consists of a two-pass Plexiglas channel. It is about 2 m long, with a square cross section of hydraulic diameter D_h = 75 mm. The walls are 15 mm thick and hermetically sealed. The U-bend connecting the two legs is interchangeable: two versions are available, one consisting of a simple circular bend of radius ratio 0.76, and the other reproducing the shape generated by the optimizer. The optimized bend was CNC-machined and polished to achieve the desired shape, which is estimated to reproduce the numerical profile with a precision of ±0.1 mm. The standard, circular bend and the optimized bend are depicted in Fig. 2. Here as in the rest of the paper, the flow goes from the left leg to the right one. Consistently with the convention adopted in the computational study, X, Y and Z refer to the spanwise, streamwise and vertical axis. A detailed description of the bends' geometries is given in Part I of the paper [16].

The operating conditions are monitored in the inlet section by static pressure taps, a traversing Pitot probe (diameter 1.5 mm) and a K-type thermocouple located $16D_h$ downstream of the settling chamber. At this location, the fluid properties, the bulk velocity and the hydraulic diameter define the Reynolds number, which is kept at 40000 for all measurements (the bulk velocity is about 8.8 m/s), as in the numerical optimization. Figure 3 illustrates a comparison of the non-dimensional measured velocity profile (across the center of the duct) with the one imposed at the entrance of the numerical domain. The latter is obtained by k-ε model letting the flow develop for $13.3D_h$ (see Part I [16]). Despite a slight asymmetry in the measured profile, a good agreement is seen.

Behind the monitoring location, the channel extends for $8D_h$ followed by the interchangeable U-bend section and finally a second leg $20D_h$ long.

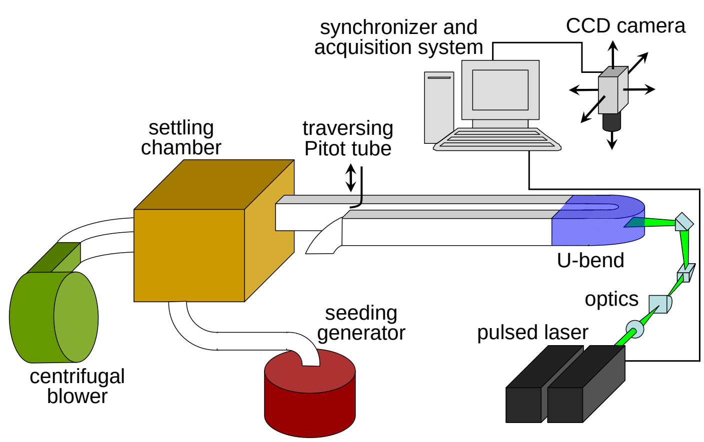

Figure 1 SCHEMATIC REPRESENTATION OF THE EXPERIMENTAL SET UP

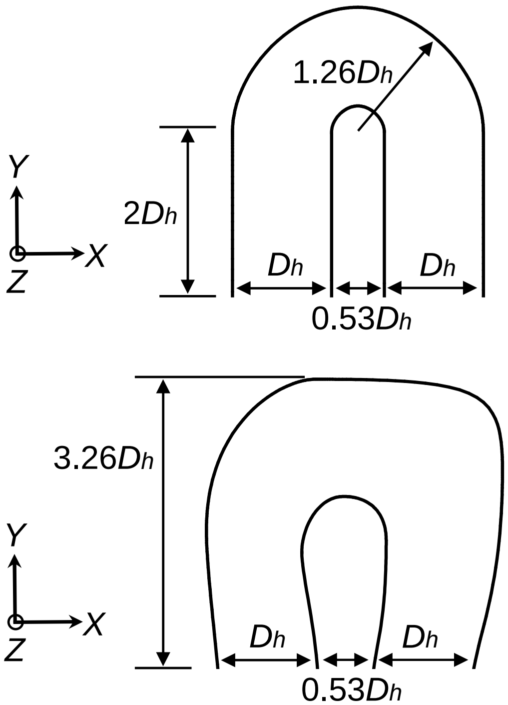

Figure 2 U-BEND GEOMETRIES FOR THE STANDARD (UP) AND OPTIMIZED (DOWN) CONFIGURATION

Pressure measurements

The cost function in the numerical optimization is the total pressure drop, as it describes the actual friction loss imposed by the U-bend. However, the experimental measurement of the total pressure at a given streamwise location of a duct requires measuring the velocity in every point of this cross-section. This implies traversing a probe (or an array of probes) along the section, which is impractical. In the present case however, the velocity distributions along the two considered cross sections are expected to be similar, as the two sections are identical and in both cases the flow is well developed. Therefore the dynamic component of the total pressure is expected to be the same at both stations. Consequently the static pressure drop between the two locations is supposed to equal the total pressure drop. This is confirmed by analyzing the data from the numerical simulation: integrating total and static pressure over the considered sections, the static pressure difference is found to match the total pressure difference within 0.5%. This justifies the experimental approach, in which the aerodynamic performance is assessed based on the static pressure drop.

Although only the U-bend shape is optimized, the effect of the geometrical modifications on the flow field can extend much further downstream. Therefore it is not sufficient to consider the pressure drop across the bend itself in order to evaluate its impact on the aerodynamic performance. The position of the cross sections considered to evaluate the pressure drop is highlighted in Fig. 4. The upstream section and

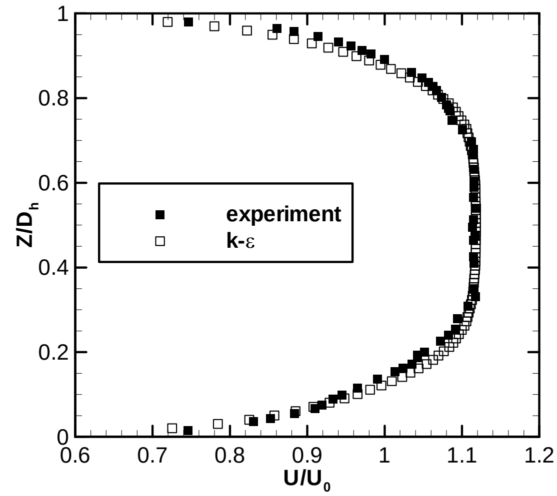

Figure 3 INLET VELOCITY PROFILE ACROSS THE CENTER OF THE DUCT: COMPARISON BETWEEN EXPERIMENTAL AND NUMERICAL RESULTS

the downstream section are located at a distance of $5D_h$ and $11D_h$ from the tip of the bend, respectively. At both locations three taps drilled in three sides of the channels are connected together, in order to provide section-averaged values. The pressure measurements are carried out by means of a differential, variable reluctance pressure transducer Validyne® DP45. The transducer is calibrated against a water manometer. The samples are acquired by means of a 16 bit A/D converter. Typical static pressure differences across the considered part of the test section range between 28 and 47 Pa.

PIV measurements

Measurements of mean velocity and Reynolds stresses are performed within the *XY* planes by means of two-dimensional PIV. For both geometries, two measurement planes are investigated (Fig. 4): one at mid channel height (Z/D_h = 0.5) and one at 2 mm from the wall (Z/D_h = 0.03).

The light source is a pulsed Nd-Yag laser, emitting a 532 nm light with an intensity of 165 mJ/pulse. The laser beam is shaped into a 1 mm thick sheet by means of a convergent spherical lens of focal length f = 1000 mm followed by a cylindrical lens of f = -60 mm. The images are acquired by a digital PCO Sensicams CCD camera with a spatial resolution of 1280 × 1024 pixels^2. A magnification factor of about 12 pixel/mm is achieved using a 55 mm Nikon objective at an aperture f/1.8. The investigated planes are divided in six to eight (depending on the bend geometry) slightly overlapping windows of about 100 × 80 mm^2. The separation time between laser pulses ranges from 60 to 120 µs, resulting in an average particle displacement of 8 to 12 pixels. Laser and camera are coordinated by a Stanford DG535 synchronizer. The sampling frequency is 2 Hz.

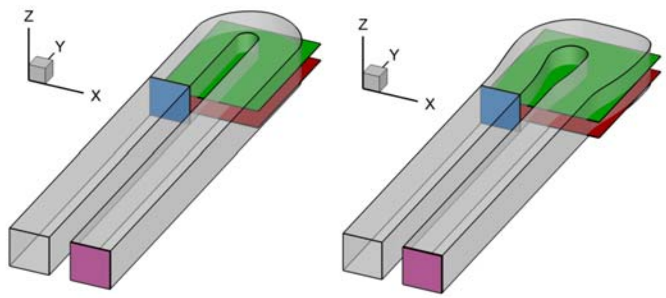

Figure 4 LOCATION OF THE MEASUREMENT PLANES: STATIC PRESSURE (BLUE AND MAGENTA) AND PIV (GREEN AND RED). THE LOCATION OF THE INLET VELOCITY PROFILE COINCIDES WITH THE ONE OF THE INLET STATIC PRESSURE MEASUREMENT (MAGENTA)

A background image is constructed by pixel-wise selection of the minimum intensity over the ensemble of the recordings and subtracted to every image, as recommended by Wereley and Meinhart [17]. The processing is realized by means of a cross-correlation based interrogation algorithm that follows an iterative multigrid approach (Scarano and Riethmuller [18]). At each refinement step the interrogation windows undergo an offset and a first order deformation. In the present case, the initial interrogation windows are 48 × 48 pixel^2. One refinement step and a 50% overlap lead to a final grid spacing of 12 × 12 pixel^2 corresponding to a resolution of 1 velocity vector/mm. The vector validation is based on the signal-to-noise ratio and the local median threshold. Rejected vectors are filled using a linear interpolation of the surrounding vectors. Mean velocity and *rms* of the velocity fluctuations are obtained averaging on 1000 image pairs.

Measurement uncertainty

The best estimation of the inlet Reynolds number uncertainty is 2%. Considering the accuracy of the transducer calibration and the *rms* of the fluctuating part of the acquired signal, the measurement of the static pressure drop is considered correct within 3%. Both estimates are determined for a 20 : 1 confidence level following the approach described by Kline and McClintock [19].

The accuracy of single PIV realizations is affected by bias errors and random errors. The first affect steadily all the velocity vectors, but can be effectively limited by an accurate choice of the measurement parameters. The second are associated to the evaluation process of the instantaneous images; they are random in nature and hence are mostly filtered out in the averaging process. Therefore, the uncertainty estimate on the mean statistics is based on the finite sampling. In the present contribution, the time-averaged quantities are computed on the basis of 1000 samples; the sampling frequency is sufficiently low to consider each realization statistically independent from the others. From the theory of signal analysis (Bendat and Piersol [20]), the uncertainties in the mean velocities and *rms* of the velocity fluctuations are estimated to be 2% and 5%, respectively, both within a confidence level of 20 : 1.

EXPERIMENTAL AND NUMERICAL RESULTS

In order to validate the proposed design approach, the results of the numerical simulations of the flow in the standard geometry and in the optimized one are compared against the experiments, both in terms of pressure drop and flow field. As the goal of the optimization is the aerodynamic performance, the information on the pressure loss would be sufficient to assess the consistency of the present approach. Nevertheless, given the complex nature of the U-bend flow, a full understanding of the numerical outcome cannot be gained without analyzing the fluid dynamics.

Pressure drop

Table 1 presents the static pressure drop for the standard and the optimized configurations, resulting from the experiments and from the numerical simulations. The values are normalized as follows:

$$\Delta P^* = \frac{P_{s,up} - P_{s,down}}{\frac{1}{2}\rho U_0^2} \tag{1}$$

where $P_{s,up}$ and $P_{s,down}$ are respectively the static pressure on the upstream and downstream measurement section, and U_0 is the bulk flow velocity measured in the section where the Reynolds number is defined. The agreement between experiments and calculations is good, and the improvement in aerodynamic performance (both measured as well as predicted) is very significant. To give a reference, the insertion of well designed turning vanes in sharp U-bend geometries provides a reduction of about 25% of the pressure drop (see Schuler at al. [21]).

	ΔP^* standard [-]	ΔP^* optimized [-]	gain [%]
experiment	1.03±0.03	0.65±0.02	36.2±3
simulation	1.01	0.63	37.6

TABLE 1 AERODYNAMIC PERFORMANCE OF THE INVESTIGATED U-BEND CONFIGURATIONS

Flow field - standard geometry

Figure 5 (up) shows streamlines and mean velocity contours measured by PIV in the U-bend region along the symmetry plane (Z/D_h = 0.5) for the standard geometry. As expected, when approaching the bend the flow accelerates near

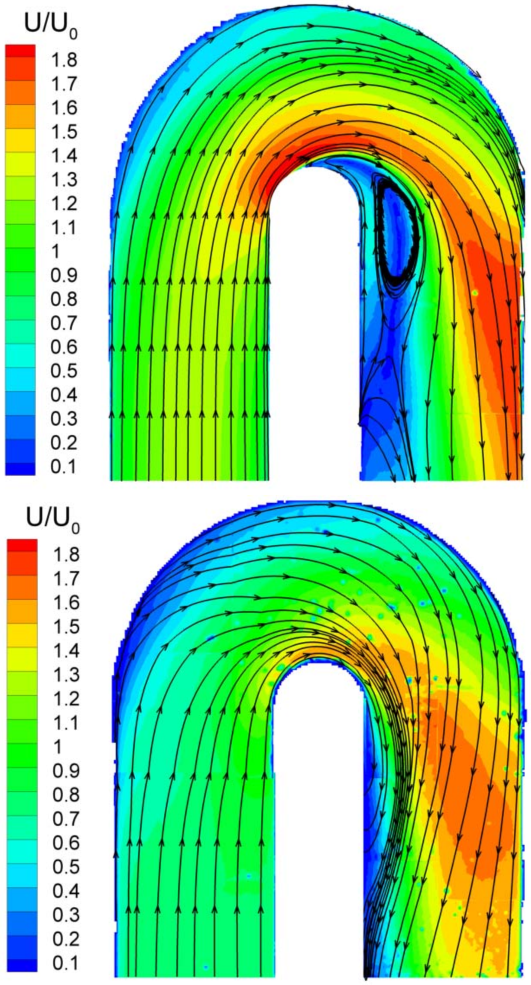

Figure 5 MEAN VELOCITY FROM PIV IN THE STANDARD GEOMETRY AT Z/Dh=0.5 (UP) AND AT Z/Dh=0.03 (DOWN).

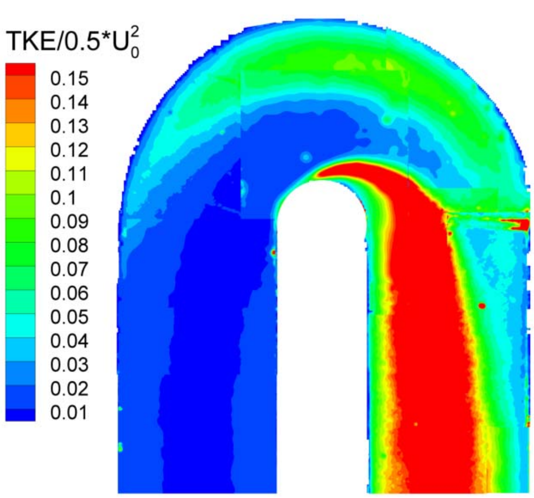

Figure 6 TURBULENT KINETIC ENERGY FROM PIV IN THE STANDARD GEOMETRY AT Z/Dh=0.5

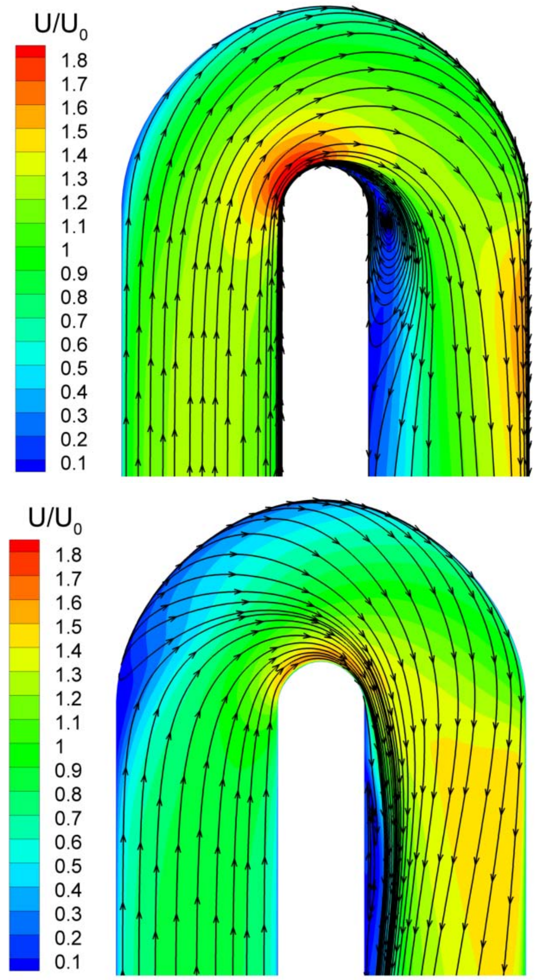

Figure 7 MEAN VELOCITY FROM CFD IN THE STANDARD GEOMETRY AT Z/Dh=0.5 (UP) AND AT Z/Dh=0.03 (DOWN).

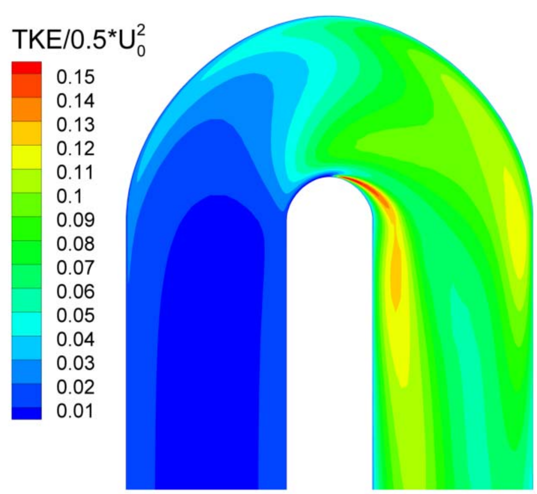

Figure 8 TURBULENT KINETIC ENERGY FROM CFD IN THE STANDARD GEOMETRY AT Z/Dh=0.5

the inner wall and decelerates near the outer wall. The streamlines along the inner wall separate just before the half of the bend, and create a large recirculation region. The latter extends for a length of about $1.6D_h$. In similar geometries, although at higher Reynolds number regimes, Monson and Seegmiller [5] found a recirculation length of about $1.5D_h$ investigating a bend of radius ratio 1, whereas Cheah et al. [6] found a length of $1.7D_h$ for a radius ratio of 0.65. The reverse flow magnitude in the recirculation bubble reaches a value as high as half of the bulk velocity, $0.5U_0$. Due to the strong curvature of the turn, the bulk of the flow reaches the second part of the outer wall, as reported in other studies of U-bend configurations with small radius ratio; however the phenomenon is far less intense in smooth than in sharp bends, where true impingements are produced (e.g. Son et. al [8]). The large extension of the recirculation bubble reduces the effective cross section and contributes to accelerate the flow even in the second half of the bend. The recirculation region displays fairly complex features: along the considered symmetry plane the bubble does not appear to terminate in a reattachment point, but rather in a source point. A similar pattern was found and discussed by Son et al. [8], who studied a sharp U-bend by PIV. They speculated that the flow was reattaching off the symmetry plane, and then the attached flows merged, creating the bifurcation pattern. Arts et al. [22] came to similar conclusions measuring a sharp U-bend flow by LDV. This view is consistent with Fig. 5 (down), which displays streamlines and mean velocity contours on a plane at Z/D_h = 0.03. The recirculation bubble is shorter than on the symmetry plane ($1.3D_h$) and ends in a typical reattachment point. In another study of a sharp U-bend, Gallo and Astarita [23] detected two couples of counter-rotating vortices generated by the turning and developing in the second leg of their channel. The merging of these vortices appeared located at the termination of the recirculation region on the symmetry plane. As no PIV measurements are available along X-Z planes, this view cannot be confirmed in the present case. The k-ε model is neither expected to yield an accurate view of the vortex interaction in such a region. However, ongoing calculations using the Reynolds stress model of Dafalias and Younis [24] (not shown here) do detect the two vortex pairs, that result in a source point at the end of the reattachment region, returning a flow pattern along the plane at Z/D_h=0.5 analogous to the one detected by PIV.

Fig. 6 displays contours of normalized turbulence kinetic energy on the symmetry plane at Z/D_h=0.5. The following definition is adopted:

$$TKE^* = \frac{TKE}{\frac{1}{2}U_0^2} = \frac{\frac{3}{4}(\overline{u^2} + \overline{v^2})}{\frac{1}{2}U_0^2} \tag{2}$$

u and w are the fluctuating parts of the velocity along the X and Z axis, respectively. The overbar indicates ensemble averaging over the 1000 acquired realizations. Following Soranna et al. [25], the 3/4 coefficient accounts for the contribution of the missing out-of-plane velocity component, assuming that it is an average of the available in-plane components. The turbulent kinetic energy is suppressed near the inner wall before the separation point. Conversely, the TKE is enhanced near the outer wall. This behavior is consistent with the well known effect of streamline curvature on turbulence properties (Bradshaw [26]). The separation, which is a strongly unsteady phenomenon, creates large production of TKE near the inner wall. Further downstream the turbulence intensity gradually diffuses across the channel, but remains strong all along the considered part of the second leg.

Figures 7 and 8 illustrate respectively the mean flow field and the turbulent kinetic energy distribution predicted by the k-ε model, and are to be compared with Figs. 5 and 6 respectively. The overall flow pattern is captured, although significant discrepancies with the PIV data exist. In Fig. 7 (up), which refers to the symmetry plane, the separation occurs later than in the experiments, and the recirculation length appears largely under-predicted, as to be expected dealing with a k-ε model (Luo and Razinsky [27]). Unlike the experimental data, there is a clear reattachment point, demonstrating how the model fails to reproduce the complexities of the streamwise vortices patterns in the downstream part of the turn. Even in the near-wall plane (Z/D_h = 0.03, Fig. 7 (down)) the similitude with the experiments is only qualitative, and the reattachment length is now over-predicted. Despite these inaccuracies, the lateral extent of the flow separation is well predicted, and consequently the computed pressure drop is very close to the experimental result (see Tab. 1).

The comparison of the turbulent kinetic energy levels predicted by the model (Fig. 8) with those measured by PIV (Fig. 6) reveals larger discrepancies. The same definition adopted for the PIV measurements (Eq. 2) is applied also to the numerical results. The inability of the model to capture the effect of curvature on the turbulence is apparent. The computation misses both the enhancement of TKE along the outer wall and its damping in the first half of the inner wall. Also the increase of turbulence due to the high shear at the separation is largely underestimated.

Flow field - optimized geometry

Figure 9 displays streamlines and mean velocity contours from PIV measurement in the symmetry plane of the optimized U-bend. With respect to the velocity field in the standard circular turn (Fig. 5 (up)), the flow acceleration is milder along the inner, convex wall. This is due to the fact that the local curvature of the inner wall, instead of passing abruptly from zero to its final value, varies smoothly along the wall contour. The inner wall is thickened and shortened compared to the standard configuration. The first part of the outer wall follows the same pattern as the inner one, and the duct section is only slightly contracting. The separation along the inner wall occurs even earlier than in the circular geometry, which is somewhat surprising. However the extension of the recirculation region is very limited, and the flow reattaches even before entering the second leg. Also the velocity magnitude of the reverse flow is decreased. The outer wall clearly plays a major role in this regard. After following an almost straight segment along the tip of the bend, it describes a fairly hasty elbow, turning the flow downstream. Despite the small local radius of curvature, no separation/recirculation is produced. On the other hand, the duct section is considerably enlarged, limiting the acceleration of the flow around the separated area and so avoiding the impinging of the flow on the outer wall. The elbow of the outer wall forces the flow downward (i.e. in negative Y direction); moreover, after enlarging at the elbow, the duct section contracts in the last part of the bend, and the consequent acceleration limits the extension of the separation bubble, particularly in the lateral (X) direction.

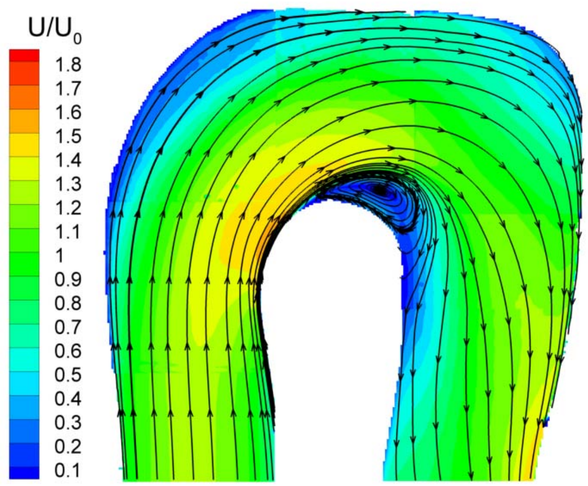

Figure 9 MEAN VELOCITY FROM PIV IN THE OPTIMIZED GEOMETRY AT Z/Dh=0.5

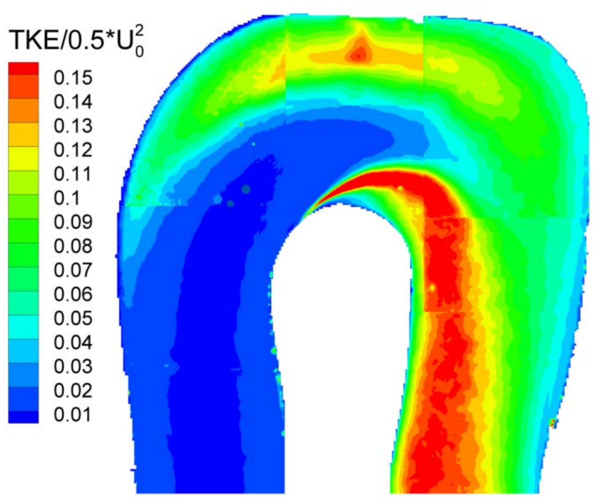

Figure 10 TURBULENT KINETIC ENERGY FROM PIV IN THE OPTIMIZED GEOMETRY AT Z/Dh=0.5

Figure 10 presents contours of turbulent kinetic energy along the symmetry plane as measured by PIV. As seen, the reduced local curvature of the inner wall in the first part of the bend yields a less pronounced inhibition of the turbulence levels with respect to the standard U-bend (see Fig. 6). The peak of TKE at separation is also much diminished in intensity and in extension, as a consequence of the limited recirculation

Figure 11 and 12 display mean flow and TKE levels in the symmetry plane from the *k-ε* calculations. The comparison with the PIV measurements confirms the obvious limits of the model in capturing the features of the reverse-flow region. The separation is predicted to happen much later than what is measured, and the lateral size of the recirculation area is largely underpredicted. Consequently, the levels of turbulent agitation are low: the peak of TKE is underestimated and the following area of diffusion is completely missed.

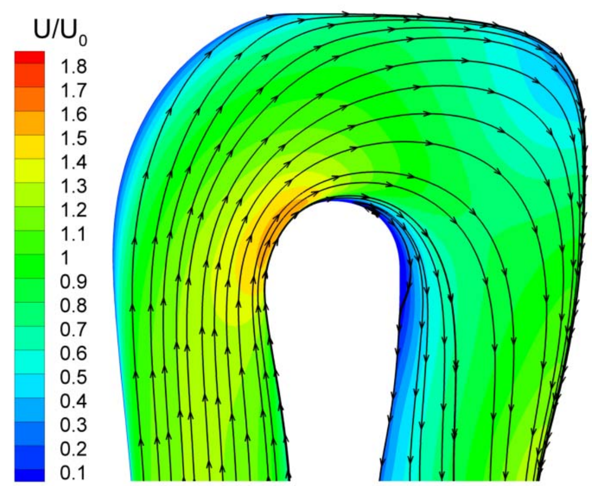

Figure 11 MEAN VELOCITY FROM CFD IN THE OPTIMIZED GEOMETRY AT Z/Dh=0.5

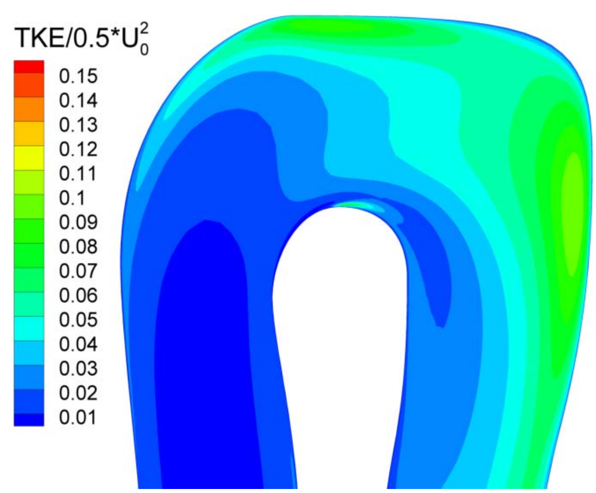

Figure 12 TURBULENT KINETIC ENERGY FROM CFD IN THE OPTIMIZED GEOMETRY AT Z/Dh=0.5

Despite the limits of the model, if one compares the features of the calculated flow in the two considered geometries (say Fig. 7 (up) and Fig. 11), the main trends revealed by the experiments are captured: the optimize U-bend yields a reduced acceleration along the concave wall and a marked decrease of the recirculation area.

Discussion

Apart from the flow details, global trends can be deduced from the presented results, which lead to *a posteriori* considerations on the 'choices' made by the optimizer. The mean radius ratio of the bend is hard to compute unambiguously in the optimized configuration, but it appears anyway larger than for the standard circular bend. This effect is the result of the enlargement of both the inner and the outer wall in the lateral direction (it is reminded here that the optimizer was not given the freedom to move further the tip of the bend). Zehner et al. [12], who optimized the contour of the divider wall of a sharp U-bend using the ice-formation technique combined with an evolutionary algorithm, found that the optimized geometry had a thicker separating wall 'filling up' the recirculation region that would have occurred otherwise. Liou and Chen [14] also found that thickening the divider wall shortens the recirculation bubble. The latter is mainly responsible for the pressure loss according to Metzger et al. [11], and its reduction is the obvious cause of the improvement in performance obtained by the proposed methodology. It is noteworthy that the thickening of the inner wall produced by the optimizer happens both in the first and in the second part of the bend, whereas improved geometries produced by experienced human designers typically display thickening only in the second leg (see e.g. Cooper [28]).

In the optimized bend the cross section, although varying along the streamwise direction, is in general wider than in the circular bend, producing lower velocity levels. Together, the increase of the radius of curvature and the reduction of the velocity leads to an overall reduction of the centrifugal force. This effect is crucial in order to limit the tendency of the flow to move away from the inner wall after separation, and therefore it helps to limit the lateral extent of the recirculation region.

The decrease of centrifugal forces in the optimized U-bend can be also deduced from Fig. 13, which shows the computed static pressure distribution along the outer wall and the inner wall at mid-span (Z/D_h=0.5). The pressure values are normalized as in Eq. 1. In the standard geometry, the higher centrifugal acceleration is balanced by a larger pressure gradient across the duct, shown by larger differences in static pressure levels between the two walls. It is remarkable how the inner wall static pressure drops abruptly due to the strong acceleration along the convex wall. The minimum corresponds to the separation point, after which the flow must face a massive adverse pressure gradient. The optimized geometry is much more efficient in this regard, as it distributes the passage loading more uniformly along its length.

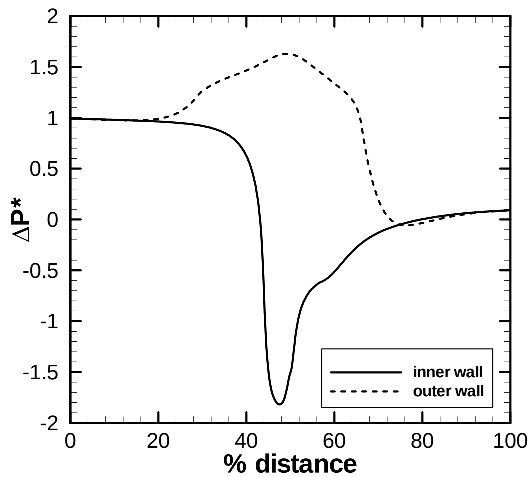

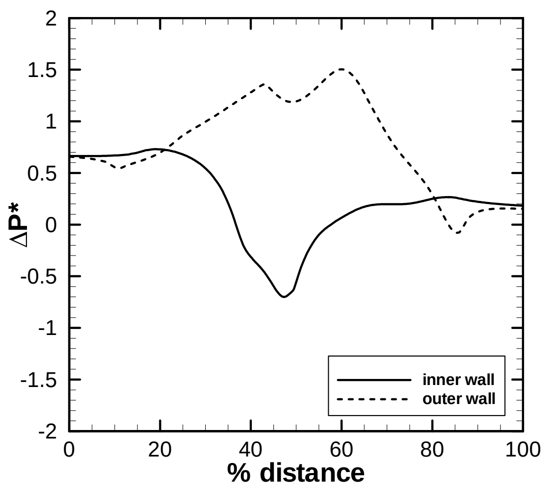

FIGURE 13 PRESSURE DISTRIBUTIONS ALONG THE INNER AND OUTER WALL AT Z/Dh=0.5 FOR THE STANDARD (UP) AND OPTIMIZED (DOWN) GEOMETRY

As seen from the mean velocity fields, the contouring of both the concave and convex walls in the optimized configuration is such that the local flow acceleration is limited. In Fig. 14 the acceleration parameter K along both walls is plotted for the two configurations, both for the experimental and the numerical results. The following definition is adopted:

$$K = \frac{\nu}{U_s^2} \frac{\partial U_s^2}{\partial s} \qquad (3)$$

s is a curvilinear abscissa that runs along the duct at $0.1D_h$ from the (outer or inner) wall, U_s is the mean velocity component along s, and ν is the flow kinematic viscosity. K is used in boundary layer studies to characterize the effect of streamwise pressure gradients, or (analogously) of the bulk velocity acceleration. To give an order of magnitude, Jones and Launder [29] proposed K=$2.5 \cdot 10^{-6}$ as a typical value above which a turbulent boundary layer relaminarizes. K is plotted in Fig. 14

against the percentage of the curvilinear abscissa; the latter is limited to the U-bend sections represented in Fig. 2. As one can see, along the inner wall the optimized profile produces an earlier and less abrupt acceleration in the first part of the bend. This is due to the reduced local curvature mentioned above. Along the outer wall the flow first decelerates and then re-accelerates. However, while in the standard geometry the acceleration continues up to the second leg, in the optimized one *K* alternates from positive to negative values, with extremal values remaining within a relatively narrow range. This control of the acceleration allows the flow to stream along the elbow without incurring in separation.

Finally it should be noticed how the optimized contour does not actually delay the separation, which is often the goal of an optimized contouring in external flows. In the present case the gain in performance is rather obtained by reducing the size of the reverse flow region, which is achieved mainly by shaping properly the concave wall. This type of approach of course can

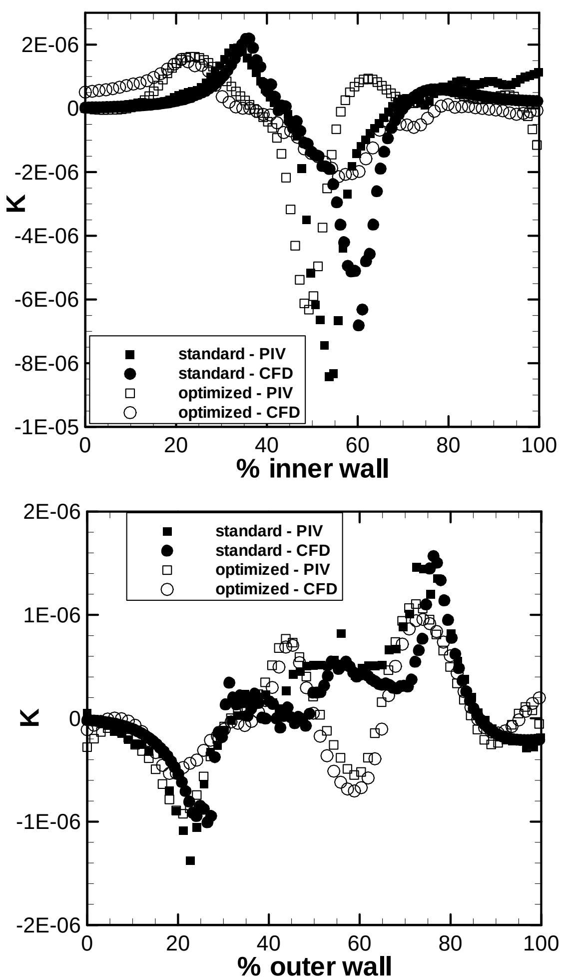

FIGURE 14 ACCELERATION PARAMETER AT Z/Dh=0.5 ALONG THE INNER WALL (UP) AND THE OUTER WALL (DOWN)

only be envisaged in internal flow configurations, in which case the possible design strategies are more numerous, and the automatic optimizer shows its utmost utility.

In the present contribution only the aerodynamic performance of the cooling channel geometry is addressed. Including the heat transfer performance would imply to tackle a multi-objective optimization problem, which is beyond the scope of the present work. Extending the analysis to the heat transfer is the natural continuation of the present study, and efforts in this direction are presently ongoing in our research group. However, it is arguable that the accuracy achievable by nowadays computational tools in terms of thermal performance is sufficient for the purpose of the present investigation. Due to the limits of turbulence models, the agreement one can obtain as for the heat transfer between experiments and RANS simulations is mostly qualitative (see the recent review of Laroche [28]). Higher fidelity simulations are not an option in optimization, due to the computational cost. On the other handRANS solvers prove to yield reliable predictions of the pressure drop. The above considerations support the present choice of focusing first on the aerodynamic performance.

CONCLUSIONS

The present contribution describes and validates an optimization methodology used to design a U-bend duct for minimum pressure drop. The geometrical features and the Reynolds number regime considered in this study are relevant to the field of turbine blade internal cooling. The method, that makes use of an evolutionary algorithm, a Navier-Stokes solver based on the k-ε turbulence model and a meta-model of it, is described in the first part of the paper [16]. In this second part the numerical results are presented both in terms of aerodynamic performance and flow field. They are compared with static pressure and velocity measurements carried out on two models, one reproducing the baseline circular geometry and the other replicating the optimized shape suggested by the algorithm. To the authors' best knowledge, this is the first study reporting the optimization of an internal cooling geometry validated by both pressure and velocity field measurements.

The optimized geometry outperforms the original circular one by about 36% in static pressure drop, which is in very good agreement with the 37% gain predicted by the numerical model. The improvement is mainly due to the reduction of the recirculation area occurring along the second half of the inner wall. Such result is the consequence of a larger radius of curvature along the inner, convex wall that limits the flow acceleration in the first half of the bend. Also beneficial is the contouring of the outer wall, which results in an overall increase of the cross section around the bend, the reduction of the velocity levels, and the decrease in radial pressure gradient.

The employed turbulence model cannot capture the effect of streamline curvature and pressure gradient on the turbulent flow field, especially in the separated region, where significant discrepancies between calculations and measurements are found. Nevertheless the major trends are well captured, which explains the significant improvement of the geometry suggested by the algorithm over the baseline circular geometry. Therefore the proposed methodology is an efficient and effective tool for improving the aerodynamic performance of internal flow configurations.

ACKNOWLEDGMENTS

The authors would like to thank Bassam Younis and Sven Schweikert for the help in the turbulence model implementation in OpenFOAM, and for the useful discussions.

NOMENCLATURE

Latin

D_h hydraulic diameter
K acceleration paramete
k turbulent kinetic energy
P static pressure
TKE turbulent kinetic energy
U velocity
s streamwise abscissa

Greek

ε dissipation of turbulent kinetic energy
ν kinematic viscosity
ρ density

REFERENCES

[1] Han J.-C., Dutta S., Ekkad S., 2000. Gas Turbine Heat Transfer and Cooling Technology. Taylor and Francis, New York.
[2] Weigand B., Semmler K., von Wolfersdorf J., 2006. Heat Transfer Technology for Internal Passages of Air-Cooled Blades for Heavy-Duty Gas Turbines. Annals of the New York Academy of Sciences 934, pp. 179-193
[3] Humphrey J. A. C, Whitelaw J. H., Yee G., 1981. Turbulent Flow in a Square Duct with Strong Curvature. J of Fluid Mech 103, pp. 443-463.
[4] Chang S. M., Humphrey J. A. C, Modavi A., 1983. Turbulent Flow in a Strongly Curved U-Bend and Downstream Tangent of Square Cross-Sections. Physico-Chemical Hydrodynamics 4, pp. 243-269.
[5] Monson D.J., Seegmiller H. L., 1992. An Experimental Investigation of Subsonic Flow in a Two Dimensional U-Duct. NASA report TM-103931.
[6] Cheah S.C., Iacovides H., Jackson D.C., Ji H.H., Launder B.E., 1996. LDA Investigation of the Flow Development Through Rotating U-ducts. J. Turbomach 118, 590-596.
[7] Liou T.-M., Chen C.-C., 1999. LDV Study of Developing Flow Through a Smooth Duct With a 180 deg Straight-Corner Turn. J Turbomach, 121(1), pp. 167-174
[8] Son S.Y., Kihm K.D., Han J.-C., 2002. PIV Flow Measurements for Heat Transfer Characterization in Two-Pass Square Channels With Smooth and 90° Ribbed Walls. Int J Heat and Mass Trans 45, pp. 4809-4822
[9] Schabacker J., Boelcs A., Johnson B. V., 1998. PIV Investigation of the Flow Characteristics in an Internal Coolant Passage with Two Ducts Connected by a Sharp 180deg Bend. ASME paper 98-GT-544.
[10] Iacovides H., Launder B. E., 1996. Computational Fluid Dynamics Applied to Internal Gas-Turbine Blade Cooling: A Review. Int J Heat and Fluid Flow 16, pp. 454-470.
[11] Metzger D. E., Plevich C. W., Fan C. S., 1984. Pressure Loss Through Sharp 180◦ Turns in Smooth Rectangular Channels. J of Engineering for Gas Turbine and Power 106, pp. 677-681.
[12] Liou T.-M., Tzeng Y.-Y, Chen, C.-C., 1999. Fluid Flow in a 180◦ Sharp Turning Duct With Different Divider Thicknesses. J Turbomach 121, pp. 569-576.
[13] Bonhoff B., Leusch J., Johnson B. V., 1999. Predictions of Flow and Heat Transfer in Sharp 180-deg Turns of Gas Turbine Coolant Channels with and without Turning Vanes, 33rd National Heat Transfer Conference, Albuquerque, NM, USA.
[14] Zehner S., Steinbrück H., Neumann S. O., Weigand B., 2009. The Ice Formation Method: A Natural Approach to Optimize Turbomachinery Components. Int J of Design & Nature 3, pp.259–272
[15] Namgoong H., Son C., Ireland P., 2008. U-bend Shaped Turbine Blade Cooling Passage Optimization. AIAA paper ISSMO 2008-5926.
[16] Verstraete T., Coletti F., Bulle J., Vanderwielen T., Arts T., 2011. Optimization of a U-bend for Minimal Pressure Loss in Internal Cooling Channels – Part I: Numerical Method. ASME paper GT2011-46541
[17] Wereley T., Gui L., Meinhart C.D., 2002. Advanced Algorithms for Microscale Particle Image Velocimetry. AIAA Journal 40, pp. 1047-1055
[18] Scarano F., Riethmuller M.L., 2000. Advances in Iterative Multigrid PIV Image Processing. Experiments in Fluids 29, pp. 51-60
[19] Kline S.J., McClintok F.A., 1953. Describing Uncertainties in Single Sample Experiments. Mechanical Engineering Journal 75, 3-8.
[20] Bendat J.S., Piersol A.G., 1986. Random Data: Analysis and Measurements Procedures. Wiley, New York.
[21] Schüler M., Zehnder F., Weigand B., von Wolfersdorf J., Neumann S.O., 2011. The Effect of Turning Vanes on Pressure Loss and Heat Transfer of a Ribbed Rectangular Two-Pass Internal Cooling Channel. J Turbomach 133, 021017 (10 pages).
[22] Arts T., Lambert de Rouvroit M., Rau G., Acton P., 1992. Aero-thermal Investigation of the Flow Developing in a 180 Degree Turn Channel. Proceedings of International Symposium on Heat Transfer in Turbomachinery, Athens.

[23] Gallo M., Astarita T., 2010. 3D Reconstruction of the Flow and Vortical Field in a Rotating Sharp ''U'' Turn Channel. Exp Fluids 48, pp. 967-982
[24] Dafalias Y. F., Younis B. A., 2009. An Objective Model for the Fluctuating Pressure Strain-Rate Correlations. J Engineering Mechanics 135, pp. 1006-1014
[25] Soranna F., Y-C. Chow, Uzol O., Katz J., 2006. The Effect of Inlet Guide Vanes Impingement on the Flow Structure and Turbulence Around a Rotor Blade. J Turbomach 128, pp. 82-95
[26] Bradshaw P., 1973. Effects of Streamline Curvature on Turbulent Flows. AGARDograph No. 169.
[27] Luo J., Razinsky E., 2009. Analysis of Turbulent Flow in 180 deg Turning Ducts With and Without Guide Vanes. Journal Turbomach 131, 21011(10 pages).
[28] Cooper B.G., 1991. Cooled Aerofoil Blade. US Patent-No. 5073086
[29] Jones W.P, Launder B.E., 1973. The Calculation of Low-Reynolds Number Phenomena With a Two-Equation Model of Turbulence. Int J Heat Mass Transfer16, 1119-1130.

